Physical Evidence that Yeast Frataxin Is an Iron Storage Protein †

ARTICLE *in* BIOCHEMISTRY · JUNE 2002

Impact Factor: 3.02 · DOI: 10.1021/bi025566+ · Source: PubMed

6 AUTHORS, INCLUDING:

Oleksandr Gakh
Mayo Clinic - Rochester
35 PUBLICATIONS **1,367** CITATIONS
SEE PROFILE

Andrew Marquis Gacy
Alion Science and Technology
27 PUBLICATIONS **1,094** CITATIONS
SEE PROFILE

R. D. Twesten
Gatan
116 PUBLICATIONS **2,903** CITATIONS
SEE PROFILE

Whyte Owen
Mayo Foundation for Medical Education and …
134 PUBLICATIONS **5,019** CITATIONS
SEE PROFILE

Physical Evidence that Yeast Frataxin Is an Iron Storage Protein†

Oleksandr Gakh,‡,§ Jiri Adamec,‡,§ A. Marquis Gacy,|| Ray D. Twesten,⊥ Whyte G. Owen,§ and Grazia Isaya*,‡,§

Departments of Pediatric & Adolescent Medicine, Biochemistry & Molecular Biology, and Pharmacology, Mayo Clinic and Foundation, Rochester, Minnesota 55905, and The Center for Microanalysis of Materials, Seitz Material Research Laboratory, Urbana, Illinois 61801

Received January 18, 2002; Revised Manuscript Received March 14, 2002

ABSTRACT: Frataxin is a conserved mitochondrial protein required for iron homeostasis. We showed previously that in the presence of ferrous iron recombinant yeast frataxin (mYfh1p) assembles into a regular multimer of ∼1.1 MDa storing ∼3000 iron atoms. Here, we further demonstrate that mYfh1p and iron form a stable hydrophilic complex that can be detected by either protein or iron staining on nondenaturing polyacrylamide gels, and by either interference or absorbance measurements at sedimentation equilibrium. The molecular mass of this complex has been refined to 840 kDa corresponding to 48 protein subunits and 2400 iron atoms. Solution density measurements have determined a partial specific volume of 0.58 cm^3/g, consistent with the amino acid composition of mYfh1p and the presence of 50 Fe-O equivalents per subunit. By dynamic light scattering, we show that the complex has a radius of ∼11 nm and assembles within 2 min at 30 °C when ferrous iron, not ferric iron or other divalent cations, is added to mYfh1p monomer at pH between 6 and 8. Iron-rich granules with diameter of 2−4 nm are detected in the complex by scanning transmission electron microscopy and energy-dispersive X-ray spectroscopy. These findings support the hypothesis that frataxin is an iron storage protein, which could explain the mitochondrial iron accumulation and oxidative damage associated with frataxin defects in yeast, mouse, and humans.

A constant supply of iron is required in the mitochondrial matrix to synthesize heme and iron−sulfur clusters. The existence of iron-binding proteins in the mitochondrial matrix has been postulated since early observations that ∼1/3 of the total mitochondrial iron is not complexed in heme or iron−sulfur clusters and is available for heme synthesis in isolated mitochondria (*1*, *2*). A mitochondria-specific ferritin has been recently identified in mammals (*3*). This protein is expressed primarily in testis and erythroblasts of patients with impaired heme synthesis and is expected to play an important role in iron management in these tissues (*3*). Frataxin represents another candidate for a role in mitochondrial iron management. This protein was first identified as the product of the Friedreich ataxia (FRDA)[1] locus (*4*) and has been shown to have a broad tissue distribution with high expression levels in heart, cerebellum, and spinal cord (*4*, *5*), the organs that undergo degeneration in FRDA patients. Potential pathogenic mechanisms by which frataxin defects lead to cardio- and neurodegeneration are suggested by studies in yeast and mouse FRDA models (reviewed in ref *6*). Inactivation of the yeast frataxin gene causes accumulation of iron in mitochondria and loss of respiratory competence (*7*−*10*). Mutant mice in which the frataxin gene is selectively inactivated in neuronal and cardiac tissues develop neurological and cardiac symptoms, defects in iron−sulfur cluster-containing respiratory enzymes, and time-dependent mitochondrial iron accumulation (*11*). Evidence of abnormal cellular iron homeostasis (*12*−*16*), increased oxidative damage (*17*−*19*), and respiratory deficits (*13*, *20*, *21*) have also been noted in tissues and cell lines derived from FRDA patients. The available experimental evidence suggests that these phenotypes may result from impaired mitochondrial iron efflux (*22*, *23*), defective biosynthesis of iron−sulfur clusters (*24*−*26*), loss of ATP synthesis (*27*), and/or disabled antioxidant defenses (*28*, *29*), with each of these conditions potentially leading to secondary mitochondrial iron overload and iron-dependent oxidative damage.

We have proposed that the involvement of frataxin in so many diverse functions could be explained if frataxin were an iron-storage protein, i.e., a protein able to keep iron in bioavailable and nontoxic form (*6*). To investigate the function of frataxin, we previously expressed the mature form of yeast frataxin (mYfh1p) in *Escherichia coli* and analyzed its ability to bind iron in vitro (*30*). Titration of mYfh1p with increasing concentrations of ferrous iron under aerobic conditions resulted in stepwise assembly of a regular multimer that sequestered ∼50 atoms of iron per subunit and exhibited an apparent molecular mass of ∼1.1 MDa as

† This work was supported by Grant AG15709 from the NIH/NIA to G.I. The Center for Microanalysis of Materials is partially supported by the U.S. Department of Energy under Grant DEFG02-96-ER45439.

* To whom correspondence should be addressed. FAX: (507) 284-1399. E-mail: isaya@mayo.edu.

‡ Department of Pediatric & Adolescent Medicine, Mayo Clinic and Foundation.

§ Department of Biochemistry & Molecular Biology, Mayo Clinic and Foundation.

|| Department of Pharmacology, Mayo Clinic and Foundation.

⊥ Seitz Material Research Laboratory.

[1] Abbreviations: FRDA, Friedreich ataxia; mYfh1p, recombinant mature form of yeast frataxin; ICP, inductively coupled plasma emission spectroscopy; DLS, dynamic light scattering; R_h, hydrodynamic radius; PAGE, polyacrylamide gel electrophoresis; STEM, scanning transmission electron microscopy; EDS, energy-dispersive X-ray spectroscopy.

10.1021/bi025566+ CCC: $22.00
Published on Web 05/03/2002

analyzed by size-exclusion chromatography and analytical ultracentrifugation (*30*). We have recently reported that the mature form of human frataxin assembles naturally during expression in *E. coli* yielding regular particles of ~1 MDa and ordered polymers of these particles that sequester ~10 atoms of iron per subunit (*31*). We have observed the presence of high-MW forms of frataxin under native conditions in yeast cells or mouse cardiac tissue, and have shown that mitochondrially produced mature frataxin binds ^{55}Fe in metabolically labeled yeast cells (*30*, *31*). In this study, we further analyze the physical properties of assembled yeast frataxin. Using gel filtration, nondenaturing polyacrylamide gel electrophoresis, and analytical ultracentrifugation, we establish that protein and iron are associated in one stable hydrophilic complex. Assembly of this complex can be detected within 2 min by dynamic light scattering, and iron-rich cores of 2−4 nm can be identified by scanning transmission electron microscopy and energy-dispersive X-ray spectroscopy of the isolated complex. These properties are consistent with a role of frataxin in iron storage.

EXPERIMENTAL PROCEDURES

Expression and Purification of mYfh1p Monomer. Purification of bacterially expressed mYfh1p monomer was carried out as described previously (*30*) with the modifications noted below. A 2-L culture of the overexpressing *E. coli* strain BL21(DE3)[pETYF-1] was used as the starting material. Bacterial cells (wet weight ~20 g) were sonicated in 20 mL of 20 mM Tris-HCl, pH 8.0, 50 mM NaCl (TN50), and the soluble fraction of the bacterial cell lysate was loaded onto a 16 mm × 50 cm column packed with Macro-Prep DEAE (Bio-Rad). The mYfh1p monomer was eluted with a 1-L linear NaCl gradient (50−550 mM) in TN50 at a flow rate of 10 mL/min. Most monomer was eluted between 310 and 380 mM NaCl. These fractions were pooled (135 mL total volume), diluted to 600 mL with deionized water, and loaded onto a Bio-Scale MT20 column (Bio-Rad) packed with Macro-Prep High Q (Bio-Rad). The mYfh1p monomer was eluted with a 0.5-L linear NaCl gradient as described above. Fractions containing mYfh1p were pooled (100 mL total volume), concentrated to 1 mL by ultrafiltration in a Ultrafree-15 device (Millipore) and loaded onto a 16 mm × 60 cm column packed with Sephacryl 300 (Amersham Pharmacia Biotech). The mYfh1p monomer was eluted with 125 mL of 10 mM HEPES−KOH, pH 7.4, 100 mM NaCl (HN100) at a flow rate of 0.6 mL/min. Fractions containing mYfh1p were pooled (15 mL total volume), concentrated, and desalted into 3 mL of 10 mM HEPES−KOH, pH 7.4, (HEPES buffer) by use of a NAP-25 column (Amersham Pharmacia Biotech). This procedure typically yielded 20−25 mg of mYfh1p with a purity of >98% as determined by SDS/PAGE. Isolated mYfh1p was stored at 4 °C and used within 2 weeks. The protein concentration was determined from the absorbance at 280 nm (ϵ_{280} = 20 000 M^{-1} cm^{-1}).

Assembly and Isolation of Iron-Loaded mYfh1p Multimer. Iron-loaded mYfh1p multimer was prepared as described previously (*30*) by incubating isolated mYfh1p monomer (typically 40 μM) with 40 equiv of ferrous iron in HEPES buffer for the indicated periods of time at 30 °C. Some assembly reactions were directly analyzed by nondenaturing PAGE as described below. In other experiments, the multimer was purified from the assembly reaction by size exclusion chromatography. In these experiments, assembly reactions (1 mL total volume) were centrifuged for 5 min at 20800*g* at 4 °C to eliminate insoluble material, and then chromatographed through a Superdex 200 column (16 mm × 50 cm; fractionation range 10−600 kDa) or a Sephacryl 300 column (16 mm × 60 cm; fractionation range 10 kDa to 1.5 MDa; exclusion limit 400 nm). The protein was eluted with HN100 buffer (100 mL at 1.5 mL/min for the Superdex 200 column, and 125 mL at 0.6 mL/min for the Sephacryl 300 column), and fractions containing the multimer were analyzed for protein concentration by SDS−PAGE and Coomassie blue staining, and for iron concentration by inductively coupled plasma emission spectroscopy (ICP). This procedure typically yielded ~0.3 mg of multimer per mg of monomer added to the assembly reaction, with an Fe/subunit ratio of ~50:1. Approximately 20% of the input protein was recovered in monomeric form and the rest in a less defined distribution of intermediate-size oligomers as reported previously (*30*).

Nondenaturing Polyacrylamide Gel Electrophoresis (PAGE). Assembly and iron loading of mYfh1p were carried out as described above. Ferritin was prepared by incubating 20 μM apoferritin (Sigma) with ferrous ammonium sulfate (2.5 mM) in HEPES buffer for 2 h at room temperature (*3*). All samples were centrifuged at 20800*g* for 5 min at 4 °C and directly analyzed by nondenaturing PAGE. The discontinuous PAGE system comprised a 3.8% stacking gel (pH 6.8) and a 7% separating gel (pH 8.9) prepared from a stock solution of 40:1.7 = acrylamide/bisacrylamide. Electrophoresis was started at 100 V, shifted to 150 V after the samples had completely entered the separating gel, and continued for an additional 90 min at 200 V after the samples had reached the bottom of the separating gel (12.5 cm total length). For Prussian Blue staining, gels were incubated with 100 mM potassium ferricyanide in 0.1 M HCl for 60 min in the dark at room temperature, they were destained with water, and dried (*31*). Scanning of dried gels was performed in a ScanJet ADF (Hewlett-Packard).

Dynamic Light Scattering (DLS). DLS measurements were carried out at different temperatures using a PDDLS/CoolBatch and PD2000/DLS system equipped with a 800 nm laser diode and a coherent detector of scattered light at an angle of 90° to the incident laser beam (Precision Detectors Inc.). Samples containing purified monomer (2.7 mg/mL) or multimer (0.1 mg/mL) in HEPES buffer were centrifuged at 20800*g* for 10 min at 4 °C to remove particulate matter before being placed in the DLS cuvette. In some experiments, monomer (200 μM) was analyzed for ~10 min at 30 °C, after which ferrous ammonium sulfate (8 mM) was added to the monomer in the DLS cuvette, and DLS measurements were continued. The diffusion constant was extracted from the autocorrelation function, and the Stokes−Einstein hydrodynamic radius (R_h) was calculated using the program PrecisionDeconvolve (Precision Detectors Inc.).

Sedimentation Equilibrium Analysis. Purified multimer was diluted with HN100 buffer or with HN100 buffer containing 46% sucrose to an absorbance at 400 nm of ~0.3 in a final volume of 0.3 mL, and was loaded into a double-sector Epon charcoal-filled 12-mm centerpiece (Beckman). Samples were centrifuged at 10 000 rpm for 2 h, and at 3000 rpm to equilibrium (48 h for multimer in HN100, and 216 h for

multimer in HN100/46% sucrose) at 19 °C in an Optima XL-I analytical ultracentrifuge (Beckman). The partial specific volume of mYfh1p/Fe-O was calculated using the equation:

$$2RT_H/(1 - \bar{v}\rho_H)\varpi_H^2 \times d \ln A_H/d(r_H^2) = 2RT_S/(1 - \bar{v}\rho_S)\varpi_S^2 \times d \ln A_S/d(r_S^2)$$

with r, ω, T, ρ, R, A, and v representing the distance from the center of rotation, angular velocity, temperature, solution density, universal gas constant, absorbance at 400 nm, and partial specific volume, respectively. The letters, H and S, denote parameters for the HN100 and HN100/46% sucrose sample, respectively. Solution densities were $\rho_H = 1.000$ g/cm^3 and $\rho_S = 1.203$ g/cm^3. The slopes [$d \ln A_H/d(r_H^2)$] and [$d \ln A_S/d(r_S^2)$] were 0.96 and 0.69, respectively. Absorbance at 400 nm vs radius data or interference vs radius data were fitted to a single component model or to a monomer−dimer model using the General Curve Fit option of the program Kaleidagraph. The best fits were selected based on chi square values, correlation coefficients, and visual inspection of the residual plots, and were used to calculate molecular masses.

Scanning Transmission Electron Microscopy (STEM) and Energy-Dispersive X-ray Spectroscopy (EDS). Purified multimer in HN100 buffer (0.1 mg of protein/mL) was diluted 5-fold with Milli-Q deionized water, concentrated by ultrafiltration, and rediluted with Milli-Q deionized water to a final iron concentration of 56 ng/μL. A sample of horse spleen ferritin containing 56 ng of iron/mL was similarly prepared. Approximately 10 μL of each sample were placed on a carbon film supported by a copper STEM grid and dried at room temperature. With no additional preparation, these samples were analyzed at 100 kV in a VG-HB501 Scanning Transmission Electron microscope with a high-resolution probe (<0.6 nm) and ~0.5 nA beam current. High-angle annular dark field images were recorded using the Gatan DigiScan system, and EDS data using the Oxford Link ISIS system.

RESULTS

DL S Analysis of mYfh1p Assembly. By use of gel filtration and analytical ultracentrifugation as well as electron and atomic force microscopy, we previously showed that titration of purified mYfh1p with increasing ferrous iron concentrations results in stepwise assembly of a regular multimer with a molecular mass of ~1.1 MDa and an Fe/subunit stoichiometry of ~50/1 (*30*). In the present study, mYfh1p assembly was analyzed directly by DLS. The mass-normalized size distribution of different mYfh1p preparations showed a narrow population of molecules with R_h of ~2 nm, consistent with the MW of mYfh1p monomer (13 783) (*30*). To initiate iron loading, purified monomer (200 μM) was incubated in HEPES buffer in a DLS cuvette and its size distribution was monitored for ~10 min at 30 °C (Figure 1). Then, ferrous ammonium sulfate (8 mM) was added to the monomer in the cuvette, the cuvette was returned to the DLS chamber, and measurements were resumed. The first R_h distribution was obtained ~2 min after iron addition. At this time, a predominant species with R_h of ~10 nm was present in the sample while monomer was no longer detected (Figure 1).

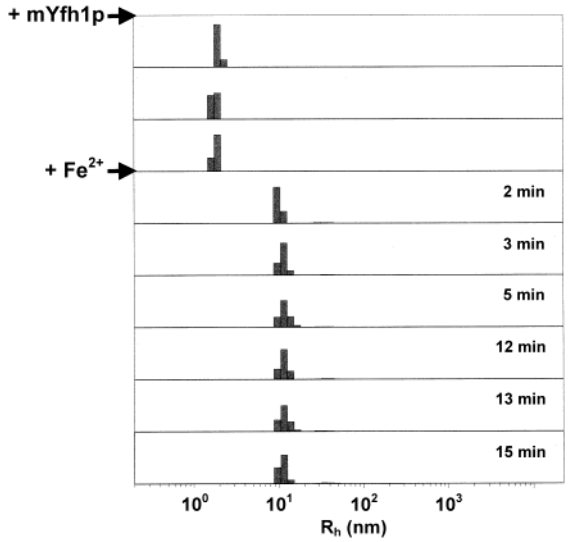

FIGURE 1: DLS analysis of mYfh1p assembly. PrecisionDeconvolve analysis of purified mYfh1p monomer (200 μM) was carried out at 30 °C before and after addition of ferrous ammonium sulfate (8 mM) as described in Experimental Procedures. The elapsed time for the iron addition step was ~2 min. Successive R_h distributions were recorded at the time points indicated. The correlator parameters were set as follows: sample time 5 ms; last channel 250; run time 1 s; accumulate 50; smoothing factor 1. A single autocorrelation function was calculated at the end of each run time, and each R_h distribution was calculated from 50 accumulated autocorrelation functions.

Small amounts (<3% of the molecules in the sample) of large aggregates with R_h of 35−60 nm were also detected (Figure 1). The DLS data were collected for an additional 15 min during which a narrow distribution of molecules with mean R_h of 11 ± 1 nm was consistently detected (Figure 1). Note that DLS could not be measured when 8 mM ferrous ammonium sulfate was added to HEPES buffer in the absence of mYfh1p, confirming that formation of the 11-nm scattering species required the presence of both mYfh1p and iron.

The DLS experiment shown in Figure 1 was repeated but the pH of the assembly reaction was varied. Results similar to those shown in Figure 1 were obtained in either HEPES buffer, pH 6 or pH 7.4, or Tris-HCl buffer, pH 8, at 25 or 30 °C. Protein and iron precipitates formed in Tris-HCl buffer, pH 9. When increasing concentrations (≤40 equiv) of Ca^{2+}, Co^{2+}, or Mn^{2+} were added to 200 μM monomer in HEPES buffer, pH 7.4, at 30 °C, the monomer did not show any tendency to self-associate as analyzed by DLS. A similar result was obtained previously when mYfh1p monomer was incubated with divalent cations and analyzed by gel filtration (*30*). Low concentrations of Fe^{3+} or Cu^{2+} (≤4 equivalents) caused protein precipitation (data not shown).

Gel Filtration and Nondenaturing PAGE Analyses of mYfh1p Assembly. We observed that the 11-nm species did not form when ferrous iron was added to mYfh1p at a temperature <20 °C. Under these conditions, intermediate-size species with R_h of 4−6 nm were detected (data not shown). This observation prompted us to investigate the kinetics of multimer formation by gel filtration. Isolated mYfh1p monomer (160 μM) was incubated with 40 Fe^{2+} equiv for 2 min at 30 or 10 °C. Each reaction was cooled to 4 °C to stop assembly and immediately analyzed by Sephacryl 300 gel filtration which was also carried out at 4

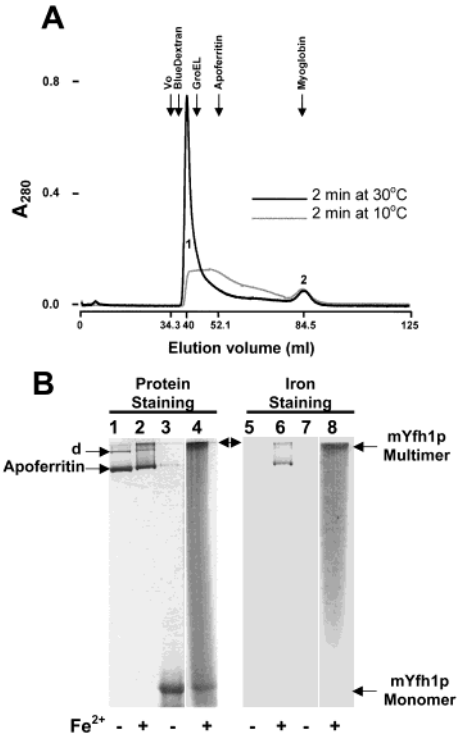

FIGURE 2: Gel filtration and nondenaturing PAGE analysis of mYfh1p assembly. (A) Purified mYfh1p monomer (160 μM) was incubated with ferrous ammonium sulfate (6.4 mM) in HEPES−KOH, pH 7.4, at 30 or 10 °C for 2 min. Each reaction was cooled to 4 °C on ice, and chromatographed through a Sephacryl 300 column at 4 °C. The black and the gray chromatograms show the elution profiles of the assembly reactions incubated at 30 and 10 °C, respectively. A_{280}, absorbance at 280 nm; V_o, void volume (34.3 mL), determined by the elution volume of formalin-fixed *Staphylococcus aureus*. Blue Dextran (2 MDa), GroEL (800 kDa), apoferritin (440 kDa), and myoglobin (17 kDa) had the following elution volumes: 36.7, 43.9, 52.1, and 83.9 mL. The elution volumes of multimer (peak 1) and monomer (peak 2) were 40 and 84.5 mL. Note that the A_{280} of peak 1 is largely due to the absorbance of Fe−O species ($\epsilon_{,280}$ = 160 000 M^{-1} cm^{-1}). (B) Duplicate assembly reactions (lanes 4 and 8) were separated by 7% nondenaturing PAGE and stained for protein with Coomassie blue and for ferric iron with Prussian blue. Purified mYfh1p monomer (lanes 3 and 7) and apoferritin (lanes 1 and 5) were used as MW standards. Ferritin (lanes 2 and 6) served as a control for ferric iron staining. The fainter band above the apoferritin band represents apoferritin dimer (d) (*32*); an additional band representing higher order polymers (*32*) is seen after iron loading of apoferritin in lanes 2 and 6. The double arrowhead shows the top of the separating gel.

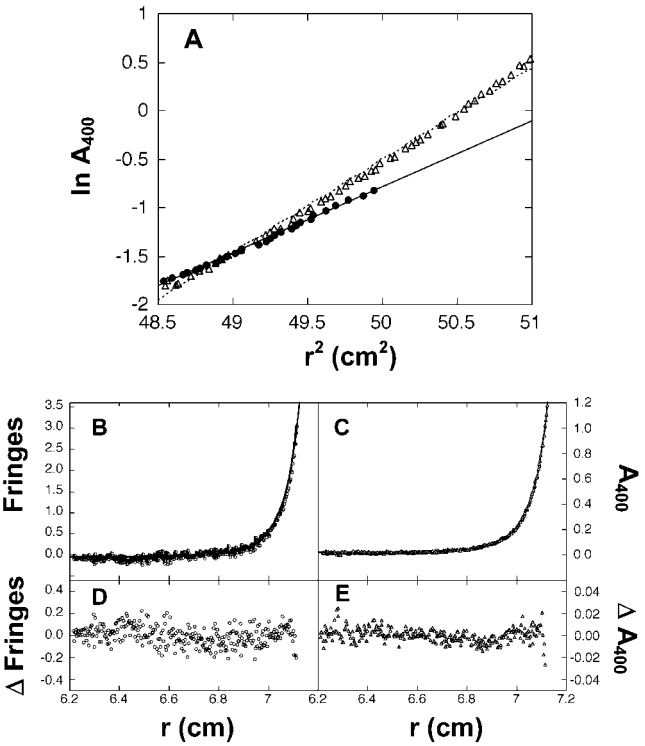

FIGURE 3: Sedimentation equilibrium analysis of mYfh1p multimer. (A) Plots of ln A_{400} vs r^2 of multimer in HN100 buffer (open triangles) and HN100 buffer containing 46% sucrose (closed circles). The slope of each line was used to determine the partial specific volume of the iron-loaded multimer as described in Experimental Procedures. (B) Interference vs r and (C) A_{400} vs r measurements of multimer at sedimentation equilibrium were fitted to an ideal monomer−dimer model as described in Experimental Procedures; (D) and (E) show the distribution of residuals.

°C. The assembly reaction that had been incubated for 2 min at 30 °C contained a major peak of ~1 MDa (Figure 2A, peak 1). This peak represents iron-loaded mYfh1p multimer as previously described (*30*). The reaction that had been incubated at 10 °C instead contained a broad distribution of species including low levels of multimer and a greater proportion of species intermediate in size between multimer and monomer (Figure 2A, peak 2). These results indicate that multimer formed during the 2 min of incubation at 30 °C prior to gel filtration, consistent with the DLS results shown in Figure 1, and was stable throughout gel filtration. In agreement with these data, DLS analysis of fractions corresponding to peak 1 revealed a homogeneous population of scatterers with R_h of ~11 nm (data not shown). Assembly reactions were also analyzed by nondenaturing PAGE. Protein staining of the assembly reaction (Figure 2B, lane 4) revealed a high-MW band that migrated above the apoferritin dimer (840 kDa) (*32*), and a low-MW band corresponding to mYfh1p monomer. A smear between these two bands suggested the presence of assembly intermediates (Figure 2B, lane 4). Prussian blue staining of the assembly reaction showed that most iron was associated with the ~1 MDa band, whereas the monomer did not contain any detectable levels of iron (Figure 2B, lane 8), as expected (*30*).

Analytical Ultracentrifugation of mYfh1p Multimer. The partial specific volume of the mYfh1p multimer was determined experimentally by subjecting multimer samples to sedimentation equilibrium in either HN100 buffer or HN100 buffer containing 46% sucrose (Figure 3A). We determined a value of 0.58 cm^3/g, which is in agreement with the theoretical partial specific volume calculated from the amino acid composition of mYfh1p and the presence of ~50 F−O equivalents per subunit (protein and iron concentrations were determined by SDS/PAGE and ICP, respectively, of isolated multimer).

A MW of ~1.1 MDa was previously determined for the iron-loaded mYfh1p multimer by sedimentation equilibrium analysis in a Beckman Prep-Scanner analytical ultracentrifuge (*30*). In this instrument, we were only able to monitor the absorbance at 280 nm which was mostly accounted for by the absorbance of Fe−O species ($\epsilon_{,280}$ = 160 000 M^{-1} cm^{-1}) present in the sample and not the absorbance of mYfh1p ($\epsilon_{,280}$ = 20 000 M^{-1} cm^{-1}). In the present study, multimer samples were analyzed in a Beckman XL-I analytical

ultracentrifuge and scanned by absorbance at 400 nm and by Rayleigh interference. Because the MW of 50 Fe−O equivalents (3,600) accounts for only 20% of the MW of the mYfh1p monomer plus 50 Fe−O equivalents (17 383), interference data should reflect primarily the sedimentation equilibrium of the multimer, while the absorbance at 400 nm should primarily reflect the sedimentation equilibrium of the associated iron, given that the absorbance at 400 nm of mYfh1p is negligible compared to that of Fe−O species. The interference vs radius plot was virtually identical to the absorbance vs radius plot (Figure 3B,C). Fitting a single component model to either the interference (correlation coefficient = 0.989) or absorbance (correlation coefficient = 0.998) data yielded the same MW value of 1.2×10^6 close to the previously determined MW of 1.1×10^6 (*30*). The agreement of the molecular masses extracted from absorbance and interference data indicates that the multimer and the iron co-sediment and are associated in a stable macromolecular complex.

Visual inspection of the residual plots of the single-component fits revealed that more than one high molecular weight species might be present (data not shown). A monomer−dimer model did fit slightly better to the data, with correlation coefficients of 0.991 and 0.999 for interference and absorbance data, respectively. The residual plots are shown in Figure 3D,E. Reliable fits could not be obtained using either monomer−polymer or two-component models (data not shown). Using the monomer−dimer fit, molecular masses corresponding to a multimer of 48 subunits (α_{48}) and a dimer of multimers of 96 subunits (α_{96}) were calculated. Specifically, molecular masses of 837 and 839 kDa were calculated for the multimer from interference data and absorbance data, respectively. The monomer−dimer fits were separated and integrated to determine the relative abundance of these two species. The α_{48} species accounted for 60% of the sample interference or absorbance, while the α_{96} species accounted for the remaining 40%.

STEM and EDS of mYfh1p Multimer. In electron micrographs, the iron associated with yeast or human frataxin appears as small electron-dense granules of ∼1−3 nm (*30*, *31*). In this study, iron-loaded mYfh1p multimer and ferritin samples were subjected to STEM. Annular dark-field imaging of the mYfh1p sample revealed a uniform dispersion of particles (Figure 4A,B) with a diameter of 2−4 nm (Figure 4D,E). EDS scans across the particles showed that they were iron rich, while the background did not contain any significant levels of iron (Figure 4D,E). Similar analyses of the ferritin sample revealed larger iron-rich particles of approximately 10−12 nm (Figure 4C,F), a difference consistent with the higher iron-binding capacity of ferritin (up to 187 Fe/subunit) (*33*) compared to mYfh1p (50 Fe/subunit).

DISCUSSION

Studies in *S. cerevisiae* and mammalian cells have shown that the protein frataxin is required for mitochondrial iron homeostasis (*7*, *8*, *11*, *16*, *22*, *34*−*36*), but the function of frataxin is not yet know. We have shown previously that both yeast and human frataxin have the ability to form regular homopolymers that can store large amounts of iron in stable form (*30*, *31*). In the present study, we have provided additional evidence that iron-dependent self-assembly of yeast frataxin yields a macromolecular complex with physical features consistent with a role in iron storage. After addition of ferrous iron to isolated mYfh1p, a species with R_h of ∼11 nm was detected within the time scale of a DLS analysis (2 min). The same species was detected by DLS analysis of multimer isolated by gel filtration (data not shown). An R_h of ∼6 nm has been reported for ferritin (440 000 MW) (*37*) and a R_h of 8.5 nm for thyroglobulin (669 000 MW) (*38*). A R_h of ∼11 nm is therefore consistent with the molecular mass of the multimer (840 kDa). This value corresponds to a hydrodynamic diameter of ∼22 nm, two times greater than the diameter we determined previously by atomic force microscopy (12.8 ± 2.1 nm) (*30*). Atomic force microscopy was conducted on multimer samples that had been dried before imaging (*30*), which should explain the smaller diameter determined by this technique. A difference of ∼50% also exists between the ferritin diameter as measured by atomic force microscopy in air (6.0 ± 1.1 nm) (*39*) and by DLS in solution (12.70 nm) (*37*).

In gel filtration experiments, ∼20% of the added protein was recovered from the column in monomeric form (Figure 2A, peak 2) regardless of the temperature at which the assembly reactions had been incubated prior to gel filtration. In DLS experiments, monomer appeared to have been fully converted to multimer after iron addition, but due to the small size of the monomer relative to the multimer, low concentrations of monomer may have not been detected by this technique. The monomeric fraction observed by gel filtration does not contain any detectable iron (*30*) and may reflect the presence of mYfh1p molecules with a protein fold incompatible with assembly. Thus, the results in Figure 2A suggest an initial step during which assembly competent monomer was assembled into oligomers of increasing size, and a subsequent step during which the oligomers were assembled into multimer without any further monomer contribution and in a temperature-dependent manner.

Our previous gel filtration studies suggested a stepwise assembly process following the pattern $\alpha \rightarrow \alpha_3 \rightarrow \alpha_6 \rightarrow \alpha_{12} \rightarrow \alpha_{24} \rightarrow \alpha_{60}$ (*30*). Assembly of a 60-mer, however, is difficult to explain according to this progression. In this study, fitting of the analytical ultracentrifugation data to a monomer−dimer model has identified two species with molecular masses of 840 kDa and 1.6 MDa, corresponding to a multimer of 48 subunits and a dimer of multimers of 96 subunits. Assembly of these species would follow the progression $\alpha \rightarrow \alpha_3 \rightarrow \alpha_6 \rightarrow \alpha_{12} \rightarrow \alpha_{24} \rightarrow \alpha_{48} \rightarrow \alpha_{96}$. A tendency to form dimers and higher order oligomers has been reported for a number of macromolecules, including ferritin (*32*), the spinach chloroplast protein, cpn21 (*40*), the oat chloroplast protein, β-glucosidase (*41*), and human frataxin (*31*). Polymerization of large protein particles has been attributed to partial denaturation of the protein shell due to mechanical stress (*37*), as may occur during the manipulations involved in analytical ultracentrifugation. Partial denaturation may expose hydrophobic regions that increase the attraction between individual particles (*37*).

We conclude that iron-dependent self-assembly of mYfh1p yields a hydrophilic macromolecule of 48 subunits that accumulates 50 iron atoms per monomer. STEM and EDS data further suggest that this iron is accumulated through a process of mineralization, as in ferritin (*33*). These results substantiate our previous work and support the hypothesis

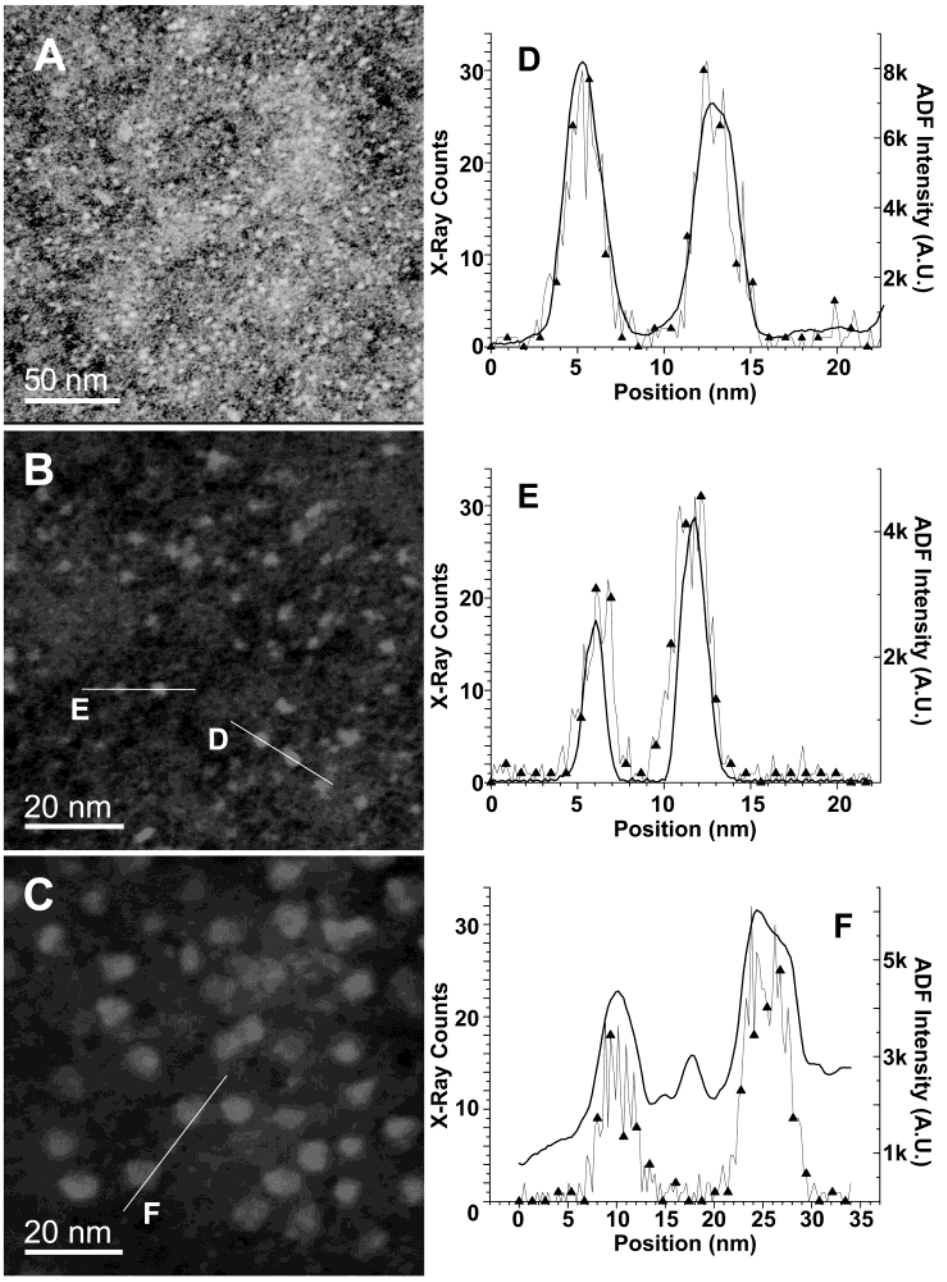

FIGURE 4: STEM and EDS analyses of iron-loaded mYfh1p multimers and horse spleen ferritin. Iron-loaded mYfh1p and ferritin multimers were prepared and diluted to a final iron concentration of 56 ng/μL. One 10-μL drop of each sample was placed on a grid and dried. With no additional preparation, these samples were analyzed by STEM and EDS as described in Experimental Procedures. Left panels show high-angle annular dark field (ADF) images of mYfh1p (A−B) and ferritin (C) multimers, and right panels (D−F) show the results of EDS scans across the particles highlighted by the white lines in panels B (mYfh1p) and C (ferritin). ▲, Fe counts; —, ADF signal; A.U., arbitrary units.

that frataxin is an iron storage protein. There is also additional evidence consistent with this view. The three-dimensional structure of human frataxin has revealed a highly conserved negatively charged surface, similar to the anionic surface involved in the iron storage mechanism of ferritin (*42*, *43*). Pastore and co-workers noted that frataxin could utilize a second, uncharged surface to assemble with itself and form a negatively charged iron-storage cavity similar to that of the *Listeria innocua* ferritin (*43*). We have recently reported that the mature form of human frataxin assembles naturally during expression in *E. coli* yielding regular particles of ~1 MDa and ordered polymers of these particles that sequester ~10 atoms of iron per subunit (*31*). We have observed the presence of high-MW forms of frataxin under native conditions in yeast cells or mouse cardiac tissue, and have shown that mitochondrially produced mature frataxin binds ^{55}Fe in metabolically labeled yeast cells (*30*, *31*). The recent identification of a mitochondrial H-ferritin in humans and other mammals (*3*) should not exclude the possibility that frataxin may act as an additional mitochondrial iron storage protein. Mitochondrial ferritin has a limited tissue distribution (*3*), whereas frataxin is ubiquitously expressed and especially in tissues with high oxygen consumption (*4*), which are the tissues that would benefit the most from a protein capable of managing iron safely within the mitochondrion. Our analysis of the assembly and iron-binding properties of frataxin should prompt further studies aimed at defining the nature and bioavailability of the stored iron, as well as

understanding the mechanism of action of this protein and the biochemical consequences of frataxin mutations.

ACKNOWLEDGMENT

We thank S. Park and H. O'Neill for help in some experiments and critical reading of the manuscript.

REFERENCES

1. Flatmark, T., and Romslo, I. (1975) *J. Biol. Chem. 250*, 6433−6438.
2. Tangeras, A. (1985) *Biochim. Biophys. Acta 843*, 199−207.
3. Levi, S., Corsi, B., Bosisio, M., Invernizzi, R., Volz, A., Sanford, D., Arosio, P., and Drysdale, J. (2001) *J. Biol. Chem. 25*, 24437−24440.
4. Campuzano, V., Montermini, L., Molto, M. D., Pianese, L., Cossee, M., Cavalcanti, F., Monros, E., Rodius, F., Duclos, F., Monticelli, A., et al. (1996) *Science 271*, 1423−1427.
5. Chew, A., Sirugo, G., Alsobrook, J. P., II, and Isaya, G. (2000) *Genomics 65*, 104−112.
6. Patel, P. I., and Isaya, G. (2001) *Am. J. Hum. Genet. 69*, 15−24.
7. Babcock, M., de Silva, D., Oaks, R., Davis-Kaplan, S., Jiralerspong, S., Montermini, L., Pandolfo, M., and Kaplan, J. (1997) *Science 276*, 1709−1712.
8. Foury, F., and Cazzalini, O. (1997) *FEBS Lett. 411*, 373−377.
9. Koutnikova, H., Campuzano, V., Foury, F., Dolle, P., Cazzalini, O., and Koenig, M. (1997) *Nat. Genet. 16*, 345−351.
10. Wilson, R. B., and Roof, D. M. (1997) *Nat. Genet. 16*, 352−357.
11. Puccio, H., Simon, D., Cossee, M., Criqui-Filipe, P., Tiziano, F., Melki, J., Hindelang, C., Matyas, R., Rustin, P., and Koenig, M. (2001) *Nat. Genet. 27*, 181−186.
12. Lamarche, J. B., Cote, M., and Lemieux, B. (1980) *Can. J. Neurol. Sci. 7*, 389−396.
13. Bradley, J. L., Blake, J. C., Chamberlain, S., Thomas, P. K., Cooper, J. M., and Schapira, A. H. (2000) *Hum. Mol. Genet. 9*, 275−282.
14. Wilson, R. B., Lynch, D. R., Farmer, J. M., Brooks, D. G., and Fischbeck, K. H. (2000) *Ann. Neurol. 47*, 659−661.
15. Scarano, V., de Cristofaro, T., De Michele, G., Salvatore, E., De Biase, I., Monticelli, A., Filla, A., and Cocozza, S. (2001) *Neurology 57*, 159−160.
16. Tan, G., Chen, L. S., Lonnerdal, B., Gellera, C., Taroni, F. A., and Cortopassi, G. A. (2001) *Hum. Mol. Genet. 10*, 2099−2107.
17. Wong, A., Yang, J., Cavadini, P., Gellera, C., Lonnerdal, B., Taroni, F., and Cortopassi, G. (1999) *Hum. Mol. Genet. 8*, 425−430.
18. Schultz, J. B., Dehmer, T., Schols, L., Mende, H., Hardt, C., Vorgerd, M., Burk, K., Matson, W., Dichgans, J., Beal, M. F., Bogdanov, M. B. (2000) *Neurology 55*, 1719−1721.
19. Emond, M., Lepage, G., Vanasse, M., and Pandolfo, M. (2000) *Neurology 55*, 1752−1753.
20. Rotig, A., de Lonlay, P., Chretien, D., Foury, F., Koenig, M., Sidi, D., Munnich, A., and Rustin, P. (1997) *Nat. Genet. 17*, 215−217.
21. Lodi, R., Cooper, J. M., Bradley, J. L., Manners, D., Styles, P., Taylor, D. J., and Schapira, A. H. (1999) *Proc. Natl. Acad. Sci. U.S.A. 96*, 11492−11495.
22. Radisky, D. C., Babcock, M. C., and Kaplan, J. (1999) *J. Biol. Chem. 274*, 4497−4499.
23. Chen, O. S., and Kaplan, J. (2000) *J. Biol. Chem. 275*, 7626−7632.
24. Foury, F. (1999) *FEBS Lett. 456*, 281−284.
25. Lutz, T., Westermann, B., Neupert, W., and Herrmann, J. M. (2001) *J. Mol. Biol. 307*, 815−825.
26. Huynen, M. A., Snel, B., Bork, P., and Gibson, T. J. (2001) *Hum. Mol. Genet. 10*, 2463−2468.
27. Ristow, M., Pfister, M. F., Yee, A. J., Schubert, M., Michael, L., Zhang, C. Y., Ueki, K., Michael, M. D., II., Lowell, B. B., and Kahn, C. R. (2000) *Proc. Natl. Acad. Sci. U.S.A. 97*, 12239−12243.
28. Chantrel-Groussard, K., Geromel, V., Puccio, H., Koenig, M., Munnich, A., Rotig, A., and Rustin, P. (2001) *Hum. Mol. Genet. 10*, 2061−2067.
29. Jiralerspong, S., Ge, B., Hudson, T. J., and Pandolfo, M. (2001) *FEBS Lett. 509*, 101−105.
30. Adamec, J., Rusnak, F., Owen, W. G., Naylor, S., Benson, L. M., Gacy, A. M., and Isaya, G. (2000) *Am. J. Hum. Genet. 67*, 549−562.
31. Cavadini, P., O'Neill, H. A., Benada, O., and Isaya, G. (2002) *Hum. Mol. Genet. 33*, 217−227.
32. Williams, M. A., and Harrison, P. M. (1968) *Biochem. J. 110*, 265−280.
33. Harrison, P. M., and Arosio, P. (1996) *Biochim. Biophys. Acta 1275*, 161−203.
34. Branda, S. S., Yang, Z. Y., Chew, A., and Isaya, G. (1999) *Hum. Mol. Genet. 8*, 1099−1110.
35. Cavadini, P., Gellera, C., Patel, P. I., and Isaya, G. (2000) *Hum. Mol. Genet. 9*, 2523−2530.
36. Foury, F., and Talibi, D. (2001) *J. Biol. Chem. 276*, 7762−7768.
37. Petsev, D. N., Thomas, B. R., Yau, S., and Vekilov, P. G. (2000) *Biophys. J. 78*, 2060−2069.
38. Hagel, L. (1999) in *Current Protocols in Protein Science* (Coligan, J. E., Dunn, B. M., Ploegh, H. L., Speicher, D. W., and Wingfield, P. T., Eds.) p 8.3.24, John Wiley & Sons, Inc.
39. Caruso, F., Furlong, D. N., and Kingshott, P. (1997) *J. Colloid Interface Sci. 186*, 129−140.
40. Baneyx, F., Bertsch, U., Kalbach, C. E., van der Vies, S. M., Soll, J., and Gatenby, A. A. (1995) *J. Biol. Chem. 270*, 10695−10702.
41. Kim, Y. W., Kang, K. S., Kim, S. Y., and Kim, I. S. (2000) *J. Mol. Biol. 303*, 831−842.
42. Dhe-Paganon, S., Shigeta, R., Chi, Y. I., Ristow, M., and Shoelson, S. E. (2000) *J. Biol. Chem. 275*, 30753−30756.
43. Musco, G., Stier, G., Kolmerer, B., Adinolfi, S., Martin, S., Frenkiel, T., Gibson, T., and Pastore, A. (2000) *Struct. Fold Des. 8*, 695−707.

BI025566+